J Mater Sci (2006) 41:4477–4483
DOI 10.1007/s10853-006-0085-9

In situ deformation of silicon nanospheres

**Julia Deneen · William M. Mook · Andrew Minor ·
William W. Gerberich · C. Barry Carter**

Received: 6 January 2006 / Accepted: 28 February 2006 / Published online: 28 June 2006
© Springer Science+Business Media, LLC 2006

Abstract As a natural response to the ongoing trend of device miniaturization, many effects of scaling on the properties of materials have become well documented. However, the mechanical properties of individual nanoparticles are not well understood and the direct observation of nanoparticle deformation has only recently been achieved. This work investigates the mechanical behavior of silicon nanospheres in the transmission electron microscope (TEM) using an in situ indentation sample holder. In situ TEM studies provide information which is not accessible by more traditional means, including particle orientation prior to deformation and the type and location of any preexisting defects. In this study, isolated nanoparticles were located and compressed between a diamond tip and a sapphire substrate. Here, the deformation behavior of individual particles is investigated and analogous strain fields between small particles are discussed.

Introduction

Understanding the mechanical properties of nanoparticles is crucial for various applications where nanoscale contacts between freestanding structures are important. For example, one of the main hurdles for the mass production of microelectromechanical systems (MEMS), whose components approach the nanoscale, is mechanical integrity issues due to the wear of rubbing surfaces [1]. Despite the growing interest in the novel properties of nanoparticles and nanostructured materials, the mechanical properties of nanoparticles are still relatively poorly understood mainly due to the practical difficulties in investigating individual particles. Though the length-scale dependence of the mechanical properties of nanoscale materials has been thoroughly investigated [2–8], those of individual nanoparticles have seen very little attention. The few studies that have interrogated individual particles [9, 10] have employed more traditional nanoindentation instruments which themselves have certain inherent limitations for nanoparticle studies. Using these methods it is impossible to accurately identify preexisting defects in the particle or to determine the orientation of the particle with respect to the loading axis, both of which are critical in quantifying mechanical behavior. To overcome these issues, the sample must be imaged in the TEM while being deformed, which requires a unique sample holder.

TEM sample holders can be designed to allow various processes to be performed while viewing the sample in the TEM. As the demand for new types of studies grows, new holders are being developed and relatively standard holders are being used in new ways. One major development in TEM holder design in recent years is the incorporation of a variety of scanning probe systems with TEM sample holders. Building a scanning tunneling microscope (STM) into a TEM holder [11] has allowed nanoscale positioning and probing of materials. In the late 1990s the STM-TEM holder was used to investigate the quantum effects in gold wires [12–14] and the properties of carbon nanotubes [15],

J. Deneen · W. M. Mook · W. W. Gerberich ·
C. B. Carter (✉)
Department of Chemical Engineering and Materials Science,
University of Minnesota, 421 Washington Avenue S.E.,
Minneapolis, MN 55455, USA
e-mail: carter@cems.umn.edu

A. Minor
National Center for Electron Microscopy, Lawrence Berkeley
National Laboratory, One Cyclotron Rd., MS 72-150, Berkeley,
CA 94720, USA

and more recently a similar STM-TEM holder has been used to probe individual semiconductor nanowhiskers [16]. In 2001 Erts et al. [17] demonstrated the capabilities of an atomic force microscope (AFM) coupled with the TEM holder by replacing the STM tip (of a STM–TEM holder) with a standard AFM cantilever, thereby allowing force measurements to be obtained while simultaneously imaging the tip and sample shape, contact area, and elastic or plastic deformation. However none of these SPM holders are designed to allow a substantial load to be applied to the sample. The in situ indentation holder, on the other hand, permits direct observation of deformation mechanisms in the TEM. The development of the holder was first described by Wall et al. in 1995 [18]. In an initial study [19], the indentation and fracture of a silicon wedge was probed by an ion etched sapphire tip in situ in a high voltage electron microscope (the Kratos 1.5 MeV). Building on this design a new nanoindentation holder was constructed for a 200 keV JEOL 200CX TEM, which allowed for both coarse and fine movement of the tip in three mutually orthogonal directions [20]. This holder has been used to investigate dislocation nucleation and motion in silicon and aluminum [21, 22]. Here an indentation holder is used to investigate the mechanical behavior of individual silicon nanospheres. However, since the nanoparticles are very small compared to the tip, the nanoparticle would more accurately be described as having been compressed.

Experimental procedure

For this study, spherical silicon nanoparticles were produced by the hypersonic plasma particle deposition (HPPD) process, which is designed for high output of particles with a controllable size distribution, chemistry, and structure [23, 24]. The particles produced by this system are spherical and occasionally contain twin boundaries and stacking faults [25–27]. Initial studies using traditional nanoindentation instrumentation also suggest that the particles have enhanced mechanical properties when compared to bulk silicon [10]. The silicon nanoparticles were deposited on a wedged sapphire substrate, which was then mounted in the TEM holder, and analyzed in a JEOL 3010 TEM operating at 300 kV. The holder is designed such that the incident electron beam is perpendicular to the loading direction of the tip and parallel to the sample substrate, such that both the tip and the sample are visible in the TEM image (Fig. 1). The diamond tip used had a nominal tip radius of 300 nm. Using this design it is possible to locate and probe an individual particle unambiguously, and the sample deformation process can be monitored in real time in the TEM using a Gatan 622 intensified television camera and videocassette recorder. The nanoparticles were compressed by a Berkovich-geometry diamond tip, doped with Boron for electron conductivity in the TEM. The tip is first coarsely positioned using manual screws, then finely positioned in the *x*, *y* and *z* directions using a piezoceramic actuator, and can be brought into the same plane as the particle by monitoring the objective lens focal difference between the tip and the chosen particle. When both the tip and the particle are in focus they are in the same plane.

Silicon nanospheres were also deposited directly on a copper TEM grid with an amorphous carbon support film. Unlike the sample prepared for the single-tilt in situ holder, this sample can easily fit in a traditional double-tilt TEM holder. Using this sample, contact between adjacent particles was investigated.

Results

With the experimental setup described it is possible to select a single nanoparticle and compress it between the sapphire substrate and the diamond tip. A single particle can be used to illustrate both elastic and plastic deformation and to demonstrate the ability to contact the same particle with the diamond tip multiple times. Controlled particle contact, causing elastic deformation, was possible as illustrated by a series of frames from a video of the particle as it was contacted, elastically deformed, and then released (Fig. 2). It was then possible to plastically deform this same particle by contacting the particle a second time and loading further, as illustrated in Fig. 3. A second

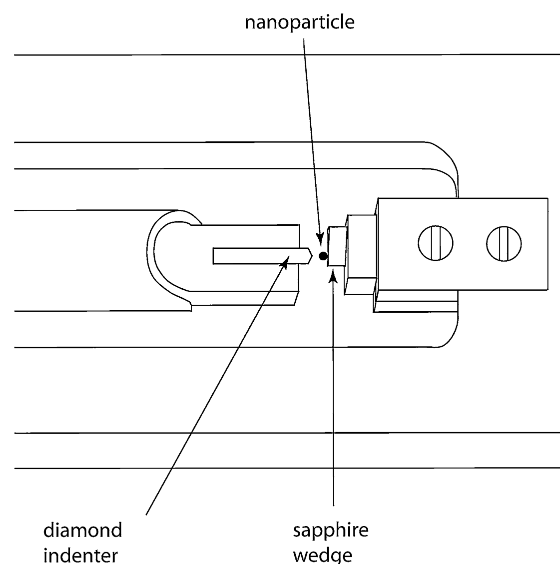

Fig. 1 Schematic of the end of the in situ indentation holder. The electron beam is perpendicular to the plane formed by the particle and the diamond tip. The nanoparticle size is exaggerated for demonstrative purposes

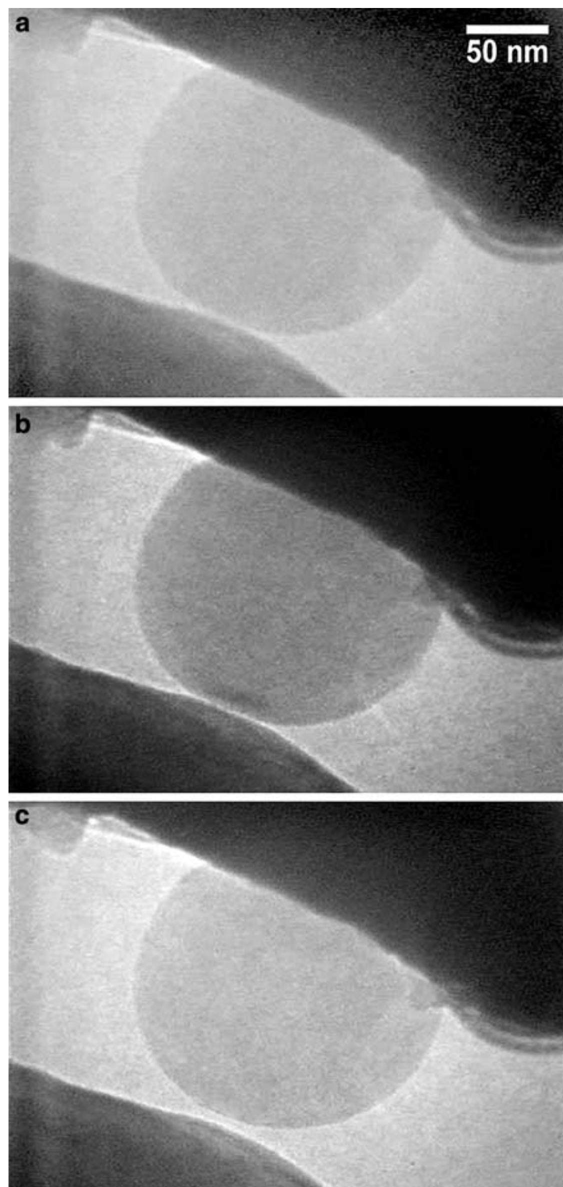

Fig. 2 Elastic contact of a nanoparticle. Prior to contact (**a**) the contrast in the particle is uniform. Strain fields can be observed as the tip contacts the particle (**b**), but are released as the tip retracts (**c**)

particle was compressed to the point of fracture, as shown here by a series of still frames extracted from a video of the deformation process (Fig. 4a–c), where the moment of fracture was determined by monitoring the bands of contrast created by the bending of lattice planes on contact by the diamond tip. In situ frame by frame analysis also demonstrated a slight widening of the particle (~5%) when comparing Fig. 4a–c. Also, aside from those formed during compression, strain fields were present when one particle directly contacted a second particle, rather than the diamond tip. If twin boundaries are present in one of the contacting particles they frequently terminate at the particle-particle contact point. Since these particles are not subject to external forces, and are therefore in equilibrium, it is possible to calculate their surface energies using well-developed contact mechanics theories.

Discussion

Elastic and plastic deformation

The first particle shown in Figs. 2 and 3 was first elastically and then plastically deformed upon contact by the tip. In Fig. 2a the particle has not yet been contacted by the tip but in Fig. 2b the tip has just come into contact with the particle and bands of contrast can be seen in the particle at the point of contact. These bands of contrast in the image are strain fields which result from the local bending of the lattice planes. As the tip was retracted (Fig. 2c) these strain fields disappeared, indicating a reversible, i.e. an elastic, deformation. This same particle was then contacted a second time, but compressed further and plastically deformed. Figure 3a shows a bright-field image of the nanoparticle prior to deformation, where the concentric thickness fringes in the particle confirm its spherical shape, and the dark-field image shown in Fig. 3b illustrates the plastic deformation induced upon further deformation.

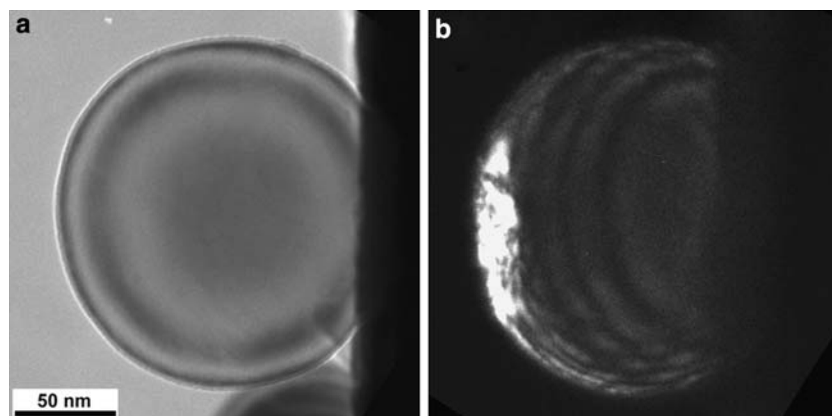

Fig. 3 (**a**) Bright field image of a particle prior to deformation. (**b**) Dark field image of the same particle after compression showing the large area of plastic deformation which has been created. This particle has been tilted slightly, but is the same particle shown in Fig. 2

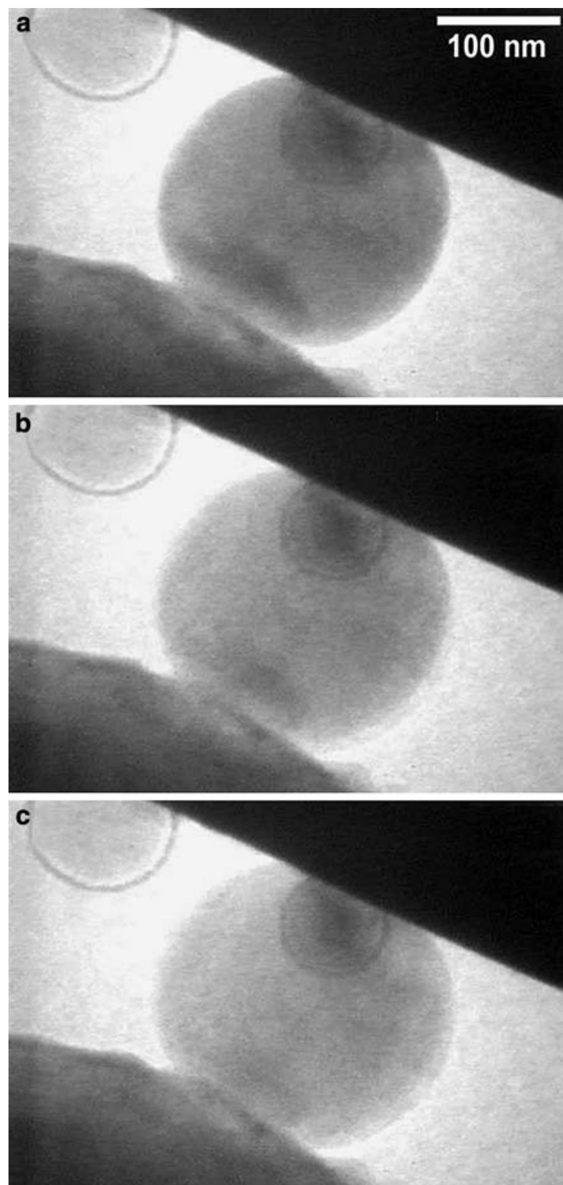

Fig. 4 Just before the moment of fracture (**a**) large strain fields are present in the particle which have partially disappeared one frame later in (**b**). In (**c**) the strain has been further released, indicating that fracture has occurred. This is not an artifact caused by the tip simply losing contact with the particle, since the particle later fractures into two pieces. Also note that the particle width increases as it is deformed over this time

The fracture of the second particle can be illustrated by a series of still frames taken from a video of the deformation event, where the time between each frame is one-thirtieth of a second (Fig. 4). In this series of frames the exact moment of fracture can be visualized. As with the previous particle, when the diamond tip was brought into contact with a single silicon nanoparticle, and strain fields are visible in both the particle (at the both the particle/substrate and particle/tip contacts) and in the diamond tip (Fig. 4a). Here the strain fields are significantly larger than those shown in the previous particle because this particle is about to fracture. The strain fields are created when the tip first contacts the particle and grow as the particle is compressed further. In Fig. 4a there is considerable strain contrast visible in the particle (prior to fracture), which is just beginning to be released in Fig. 4b, and has further decreased in Fig. 4c. The strain release in that fraction of a second indicates that fracture has occurred. Also, the particle appears progressively wider as it is compressed, having increased its apparent diameter by 10 nm in only one fifteenth of a second, while the smaller undeformed particles sitting approximately ~200 nm away in the camera's plane of view have not changed. (These smaller particles do not interfere with deformation since they lie in different planes, as indicated by the Fresnel fringes.) Figure 5 illustrates that the strain release is not an artifact caused by the tip having lost contact with the particle, as the particle has fractured into two pieces.

After determining the moment of fracture it then becomes possible to determine other parameters including the total amount of deformation, the amount of strain prior to fracture, and the contact area at fracture. This particle was compressed nearly 30 nm prior to fracture, equating to a compressive strain of 13% in the center of the contact. While strains of this magnitude are uncommon for brittle materials such as bulk silicon, micro- and nanoscale structures of single crystal silicon do fatigue and fail similar to metallic materials [28].

Particle–Particle Contacts

Strain fields observed in nanoparticles are not limited to those formed due to compression. Strain fields are also present when one particle is in direct contact with a second particle. Since it is more energetically favorable for two contacting particles to contact across an area than at a single point due to surface forces, strain fields generated from elastic deformation form at these contacts. A strain field is created which is compressive at the center of the contact and tensile towards the edges. This is equivalent to the initial instant of contact in the compression experiments detailed above. Figure 6 shows one large particle contacting two slightly smaller particles with strain fields present at both contacts. These particles are under no externally applied loads, and thus at equilibrium. Similar fields have been observed in various nanoparticle systems including gold, cobalt, nickel and iron [29–32]. These observed strain fields can provide quantitative information concerning the particles as described by Thölén and Yao [31]. They apply the Johnson–Kendall–Roberts (JKR) model [33] to estimate the particles' contact stress distribution and surface energy [34]. JKR analysis modifies the standard Hertzian contact of two elastic spheres by accounting for surface

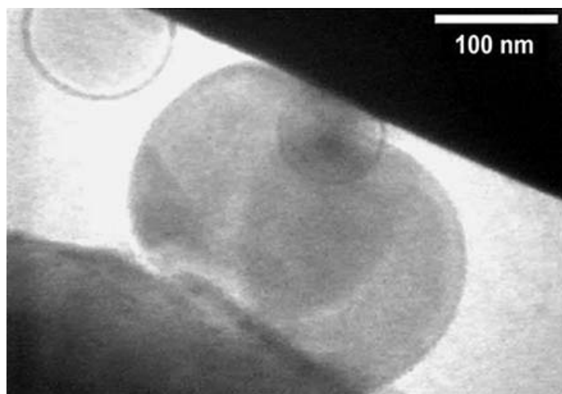

Fig. 5 After further compression the particle has unambiguously fractured into two pieces

energy, which increases contact area at low loads and explains particle-particle adhesion at zero load. Since there is no external load, the appropriate relationship, as shown in Appendix A, is

$$\gamma_{\mathrm{eff}} = 2\gamma_{\mathrm{s}} - \gamma_{\mathrm{gb}} = \frac{Ea_{\mathrm{c}}^{3}}{9\pi R^{2}(1-v^{2})}, \tag{1}$$

Here, γ_s is the surface energy of the sphere, E is the elastic modulus, v is Poisson's ratio and R is the effective radius of the two particles calculated from Hertzian contact mechanics as

$$\frac{1}{R} = \frac{1}{R_1} + \frac{1}{R_2}. \tag{2}$$

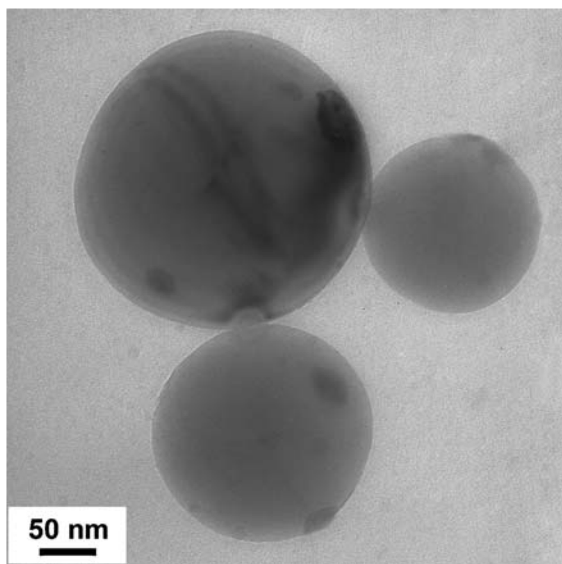

Fig. 6 A larger nanoparticle is contacting two smaller particles; strain fields are present at each contact

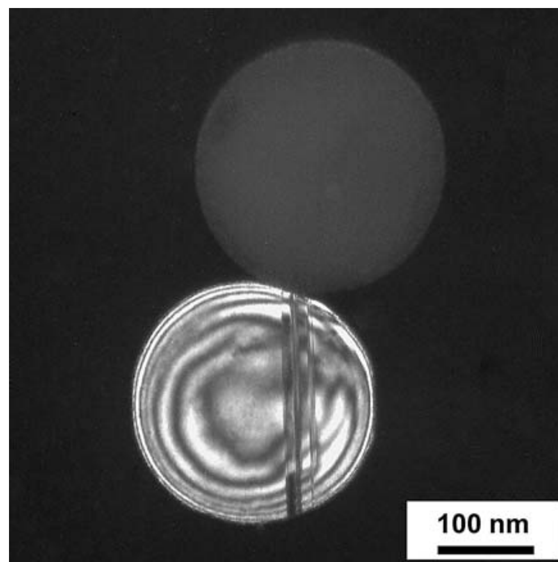

Fig. 7 Two contacting particles, which have come into contact at a twin boundary. There is no noticeable strain at the contact point

Equation (1) reduces the effective surface energy by a factor of four when compared to that obtained from Eq. (3) in the Appendix, but of course the decrease in a_c to a_{adh} compensates for that [35]. In Fig. 6, the two particles have radii of R_1 = 133 nm, and R_2 = 98 nm, giving an effective radius of R = 56.4 nm. The contact radius due to adhesion between the particles is measured to be approximately 14 nm. This gives a value for γ_s of 2.35 J/m^2 assuming standard values for elastic modulus and Poisson's ratio of silicon to be 160 GPa and 0.218, respectively. This is a realistic assessment of particle surface energy since in general, nanoparticles can have energies up to an order of magnitude higher than their bulk counterparts [36], and 2.35 J/m^2 neglects the grain boundary energy, γ_{gs}, and is close to the accepted value for bulk silicon of 1.56 J/m^2.

Twinning is also occasionally observed in the nanospheres, and twins which terminate at particle-particle contact points are observed frequently (Fig. 7), a phenomenon also observed in similar systems of metallic particles [30]. One explanation suggests that the contact stresses between particles could be large enough to create deformation twins [30]. In the present system it is more likely that the large majority of these twins are formed during the growth process. The twin forms a local flat region in an otherwise spherical particle. The twinned region thus increases the area of contact with neighboring particles such that they contact here rather than at another point on the particle. This is consistent with the lack of strain fields at the contact point in the case of the twinned particle.

Conclusions

The future of nanoscale characterization is now looking to in situ TEM studies for determining the properties of nanoparticles, since only then can the phenomenon in question be observed directly. This study illustrates the use of an in situ indentation TEM holder in investigating the mechanical behavior of silicon nanoparticles. In the silicon particles both elastic and plastic deformation have been observed, and the exact moment of nanoparticle fracture has been illustrated. Additionally, particle-particle contacts at equilibrium provide a means to evaluate the nanoparticle surface energy by the application of traditional contact mechanics concepts. The approaches described here can readily be extended to particles of various sizes, geometries and chemistries.

Acknowledgments This research was funded through NSF grant number CMS0322436. The authors acknowledge support of the staff and facilities at the National Center for Electron Microscopy. We would also like to thank Prof. Steven Girshick and the HPPD research group for provision of the particles, and Prof. Anders Thölén and Dr. Martina Luysberg for helpful discussions.

Appendix A

For analyzing the surface energy between two spheres as shown in Fig. 6, it was first considered that the result represented by Johnson's Equation (5.51) in Ref. [35] could be utilized directly given by

$$\gamma_{\text{eff}} = 2\gamma_s - \gamma_{gb} = \frac{4E^* a^3}{9\pi R^2} \tag{3}$$

where γ_{gb} is a grain boundary energy. In using the value of R equal to 56.4 nm from Eq. (2) this gave too large a result since the contact radius used, a_c, was that at zero load while Eq. (3) is appropriate to a_{adh} at the maximum negative tensile load necessary to separate the particles (represented by Pt. B in Fig. 5.8, Ref. [34]). Using the JKR result [33, 35],

$$a^3 = \frac{PR}{K}\left[1 + \frac{3\pi\gamma_{\text{eff}}R}{P} + \sqrt{\frac{6\pi\gamma_{\text{eff}}R}{P} + \frac{(3\pi\gamma_{\text{eff}}R)^2}{P^2}}\right] \tag{4}$$

and setting $P = 0$ appropriate to Fig. 6, one obtains

$$a_c^3 = \frac{6\pi\gamma_{\text{eff}}R^2}{K}. \tag{5}$$

With the definition of $K = (2/3)\left(E/(1-\nu^2)\right)$, this becomes

$$\gamma_{\text{eff}} = \frac{Ea_c^3}{9\pi(1 - \nu^2)R^2} \tag{6}$$

which is Eq. (1) as utilized in the main text. Equations (3) and (6) are consistent with Johnson's Fig. 5.8, Ref. [35].

References

1. Tanner DM, Smith NF, Irwin LW, Eaton WP, Helgesen KS, Clement JJ, Miller WM, Walraven JA, Peterson KA, Tangyunyong P, Dugger MT and Miller SL Tech. Report No. SAND2000–0091 (Sandia National Laboratory, 2000)
2. Arzt E (1998) Acta Mater 46:5611
3. Brenner SS (1956) J Appl Phys 27:1484
4. Brenner SS (1957) J Appl Phys 28:1023
5. Gryaznov VG, Polonsky IA, Romanov AE, Trusov LI (1991) Phys Rev B 44:42
6. Gryaznov VG, Trusov LI (1993) Prog Mater Sci 37:289
7. Veprek S (1997) Thin Solid Films 297:145
8. Veprek S, Mukherjee S, Mannling HD, HE JL (2003) Mater Sci Eng A 340:292
9. Mook WM, Jungk JM, Cordill MJ, Moody NR, Sun Y, Xia Y, Gerberich WW (2004) Z Metallkd 95:416
10. Gerberich WW, Mook WM, Perrey CR, Carter CB, Baskes MI, Mukherjee R, Gidwani A, Heberlein JVR, Mcmurry PH, Girshick SL (2003) J Mech Phys Solids 51: 979
11. Spence JCH (1988) Ultramicroscopy 25:165
12. Ohnishi H, Kondo Y, Takayanagi K (1998) Surf Sci 415:L1061
13. Kizuka T (1998) Phys Rev Lett 81:4448
14. Kizuka T, Yamada K, Deguchi S, Naruse M, Tanaka N (1997) Phys Rev B Condens Matter Mater Phys 55:R7398
15. Cummings J, Zettl A (2000) Science 289:602
16. Larsson MW, Wallenberg LR, Persson AI, Samuelson L (2004) Microsc Microanal 10:41
17. Erts D, Lohmus A, Lohmus R, Olin H (2001) Appl Phys A: Mater Sci Process 72:S71
18. Wall MA, Barber TW, Dahmen DU (1995) Paper presented at the 53rd Annual MSA Meeting, Kansas City, Missouri
19. Wall MA, Dahmen U (1997) Microsc Microanal 3(Suppl. 3):593
20. Stach EA, Freeman T, Minor AM, Owen DK, Cumings J, Wall MA, Chraska T, Hull R, Morris JW, Zettl A, Dahmen U (2001) Microsc Microanal 7:507
21. Minor AM, Morris JW, Stach EA (2001) Appl Phys Lett 79:1625
22. Minor AM, Lilleodden ET, Stach EA, Morris JW (2002) J Electron Mater 31:958
23. Rao NP, Lee HJ, Kelkar M, Hansen DJ, Heberlein JVR, Mcmurry PH, Girshick SL (1997) NanoStruct Mater 9:129
24. Rao NP, Tymiak N, Blum J, Neuman A, Lee HS, Girshick SL, Mcmurry PH, Heberlein J (1998) J Aerosol Sci 29:707
25. Perrey CR, Lentzen M, Carter CB (2003) Microsc Microanal 9:394
26. Perrey CR, Carter CB, Bentley J, Lentzen M (2003) Microsc Microanal 9:412

27. Perrey CR, Carter CB, Lentzen M (2003) Microsc Microanal 9:958
28. Muhlstein CL, Brown SB, Ritchie RO (2001) J MEMS 10:593
29. Easterling KE, Thölén AR (1972) Acta Metall 20:1001
30. Thölén AR (1990) Phase Transitions 24–26:375
31. Thölén AR, Yao Y (2003) J Colloid Interface Sci 268:362
32. Thölén AR (2006) J Mater Sci (This issue)
33. Johnson KL, Kendall K., Roberts AD (1971) Proc R Soc London Ser A 324:301
34. Johnson KL (1958) Br J Appl Phys 9:199
35. Johnson KL (1985) Contact mechanics. Cambridge University Press
36. Nanda KK, Maisels A, Kruis EE, Fissan H, Stappert S (2003) Phys Rev Lett 91:106102/1